Received: 1 June 2020 | Revised: 29 October 2020 | Accepted: 2 November 2020

DOI: 10.1002/acm2.13106

RADIATION ONCOLOGY PHYSICS

WILEY

Effect of an integral quality monitor on 4-, 6-, 10-MV, and 6-MV flattening filter-free photon beams

Trang Hong Thi Nguyen[1] | Haruna Yokoyama[2] | Hironori Kojima[2] | Naoki Isomura[2] | Akihiro Takemura[3] | Shinichi Ueda[2] | Kimiya Noto[2]

[1]Division of Health Sciences, Graduate School of Medical Sciences, Kanazawa University, Kanazawa, Japan

[2]Department of Radiological Technology, Kanazawa University Hospital, Kanazawa, Japan

[3]Faculty of Health Sciences, Institute of Medical, Pharmaceutical and Health Sciences, Kanazawa University, Kanazawa, Japan

Author to whom correspondence should be addressed. Akihiro Takemura
E-mail: at@mhs.mp.kanazawa-u.ac.jp.

Abstract

Purpose: To investigate the effect of an integral quality monitor (IQM; iRT Systems GmbH, Koblenz, Germany) on 4, 6, 10, and 6-MV flattening filter-free (FFF) photon beams.

Methods: We assessed surface dose, $PDD_{20,10}$, $TPR_{20,10}$, PDD curves, inline and crossline profiles, transmission factor, and output factor with and without the IQM. PDD, transmission factor, and output factor were measured for square fields of 3, 5, 10, 15, 20, 25, and 30 cm and profiles were performed for square fields of 3, 5, 10, 20, and 30 cm at 5-, 10-, and 30-cm depth.

Results: The differences in surface dose of all energies for square fields of 3, 5, 10, 15, 20, and 25 cm were within 3.7% whereas for a square field of 30 cm, they were 4.6%, 6.8%, 6.7%, and 8.7% for 4-MV, 6-MV, 6-MV-FFF, and 10-MV, respectively. Differences in $PDD_{20,10}$, $TPR_{20,10}$, PDD, profiles, and output factors were within $\pm$1%. Local and global gamma values (2%/2 mm) were below 1 for PDD beyond d_{max} and inline/crossline profiles in the central beam region, respectively. The gamma passing rates (10% threshold) for PDD curves and profiles were above 95% at 2%/2 mm. The transmission factors for 4-MV, 6-MV, 6-MV-FFF, and 10-MV for field sizes from 3×3 to 30×30 cm^2 were 0.926–0.933, 0.937–0.941, 0.937–0.939, and 0.949–0.953, respectively.

Conclusions: The influence of the IQM on the beam quality (in particular 4-MV X-ray has not verified before) was tested and introduced a slight beam perturbation at the surface and build-up region and the edge of the crossline/inline profiles. To use IQM in pre- and intra-treatment quality assurance, a tray factor should be put into treatment planning systems for the dose calculation for the 4-, 6-, 10-, and 6-MV flattening filter-free photon beams to compensate the beam attenuation of the IQM detector.

KEY WORDS

beam quality, integral quality monitor (IQM), photon energy

1 | INTRODUCTION

Quality assurance (QA) plays an important role in minimizing and preventing errors in radiation therapy. Dosimetric evaluation for treatment plans has routinely used ionization chambers, thermoluminescent dosimeters, optically stimulated luminescent dosimeters, and films as conventional QA techniques.[1–4] However, the disadvantage of these QA devices is that they have only been used for offline verification and cannot predict any unexpected errors in vivo dosimetry. Moreover, the gamma passing rates were reported to be insufficient for prediction of dose errors in QA of intensity-modulated radiation therapy.[5,6] Beam output should be verified during treatment to avoid potential treatment errors such as equipment failure and wrong plan selection.[7,8] Therefore, some advanced *in vivo* QA methods were introduced to increase the dosimetric accuracy in vivo dosimetry such as point dosimeters, electronic portal imaging device dosimetry (EPID), transmission detectors, linac log file analysis, and dose accumulation methods.[9–19] The point dosimeters and EPID are sensitive to linac and patient errors.[20] Transmission detectors monitor linac performance with high sensitivity in real time.[20] Linac log file analysis is sensitive to plan corruption errors.[20] Dose accumulation methods are used to evaluate intrafraction movements and the multileaf collimator (MLC) tracking systems.[20]

A type of new transmission detector called an integral quality monitor (IQM) has been commercialized by iRT Systems GmbH, Koblenz, Germany. The IQM is mounted on a linear accelerator (linac) gantry head and uses an independent system monitor to provide on-line beam monitoring that can detect treatment delivery errors that exceed an acceptance level.[9] The IQM is a wedge-shaped ionization chamber with a continuous spatial resolution and the large sensitive volume that can detect a small range of systematic MLC error compared with 0.6-cc Farmer chamber (PTW 30013, Freiburg, Germany), Delta4 (ScandiDos, Uppsala, Sweden), and 2D-array seven29 (PTW, Freiburg, Germany).[21] However, when the IQM is placed in the beam path, it was reported that the IQM affected to be small yet statistically significant photon beam properties with the increase in the surface dose and beam attenuation of 6-, 10-, 15-, 18-MV, and 6-, 10 -MV flattening filter-free (FFF) X-ray beams.[22] With respect to the effect of IQM on beam quality, Casar et al.[22] evaluated the surface dose, difference in the ratio of percentage depth dose at depths of 20 and 10 cm ($PDD_{20,10}$), and transmission factors for field sizes from 1×1 to 20×20 cm^2 for 6-, 10-, 15-, and 18-MV and for two FFF photon beams (6- and 10-MV FFF). Islam et al.[9] evaluated the surface dose, the profiles at 1.5 and 10 cm depths for 30×30 cm^2 field and percent depth dose for 10×10 and 30×30 cm^2 fields, and transmission factor for a field size of 10×10 cm^2 for 6- and 18-MV X-ray beams. Hoffman et al.[23] evaluated the surface dose, the profiles at 10 cm depth for 30×30 cm^2 field and percent depth dose for 10×10 cm^2 fields, and transmission factor for field sizes of 1×1 and 10×10 cm^2 for 6-, 10- and 15-MV beams. As a novelty of this manuscript, we furnish a broad and complete view of the beam perturbation induced by IQM by evaluating the differences in the surface and build-up region dose, $PDD_{20,10}$, tissue phantom ratio at depths of 20 and 10 cm ($TPR_{20,10}$), percentage depth dose (PDD) curves, inline and crossline profiles, transmission factor, and output factor measured with and without the IQM for field sizes of 3×3, 5×5, 10×10, 15×15, 20×20, 25×25, and 30×30 cm^2 for 4-, 6-, 10-, and 6-MV flattening filter-free (FFF) X-ray beams.

The previous studies evaluated the influence of the IQM on photon energies of Elekta linacs (Synergy, Precise, and Versa HD (Elekta AB, Stockholm, Sweden)) with 6-MV low-energy photons, 10-MV mid-energy photons, and 15- and 18-MV high-energy photons.[9,22,23] However, in this study, we used an Elekta Infinity linac (Elekta AB, Stockholm, Sweden) with 4-MV low-energy photons, 6-MV mid-energy photons, and 10-MV high-energy photons. In Japan, there is basically a difference in the number of FFF beams between Elekta Infinity and Elekta Versa HD. The Elekta Versa HD has two FFF beams with 10- and 6-MV FFF X-ray beams whereas the Elekta Infinity only selects one of the FFF beams. Outside Japan, the specifications of linac may differ slightly. The Elekta Infinity with Agility MLC (160 leaves with 1 cm leaf width) can be installed depending on the country. In Japan, the 4-MV X-ray beam is used as low-energy photon instead of 6-MV X-ray beam because the 4-MV X-ray beam is routinely used for breasts with small configuration in Japan whereas the 6-MV X-ray beam or higher energy photon is used for large-size breasts in US and Europe.[24] Therefore, the beam shaping inside Elekta linac in Japan is different from global Elekta linac. The 4-MV beam of Japan and 6-MV beam of global Elekta were produced with the combination of the primary collimator in the open position and secondary filter at the position of the low-energy X-ray filter, as shown in Table 1. The 6-MV beam of Japan and 10-MV beam of global Elekta were delivered at the open position of the primary collimator and secondary filter at the mid-energy X-ray filter. The 10-MV beam of Japan and 15-MV beam of global Elekta were produced with the combination of the primary collimator at the filter position and secondary filter at the mid-energy X-ray filter. Because the configuration of Elekta linacs depends upon the situation of each country, the evaluation of effect of the linac variation for photon beam is necessary and the results obtained for the 6- and 10-MV beams in this study should be comparable with published papers.

TABLE 1 Difference of photon delivery system between the Elekta Linac in Japan and the global Elekta Linac for low-, mid-, and high-energy photons.

Energy Variations	Low-energy	Mid-energy	High-energy
Primary collimator	Open position	Open position	Filter position
Secondary filter	Low-energy X-ray filter	Mid-energy X-ray filter	Mid-energy X-ray filter
Global	6 MV	10 MV	15 MV
Japan	4 MV	6 MV	10 MV

2 | MATERIALS AND METHODS

2.A | Measurements of PDD curves and inline/crossline profiles

The IQM detector is attached to a gantry head of the Elekta Infinity linac. All measurements were carried out on the Elekta Infinity with an Agility MLC system (160 leaves with 0.5 cm leaf width) (Elekta AB, Stockholm, Sweden). PDD with and without the IQM was measured from a depth of 30 cm up to the surface water in a cylindrical 3D Scanner v.3.3.1 water phantom (Sun Nuclear, Melbourne, FL) using a 0.125-cm^3 SNC125c chamber (Sun Nuclear, Melbourne, FL) and SNC Dosimetry™ scanning software v.3.4.0.26814 (Sun Nuclear, Melbourne, FL) at a source-to-surface distance (SSD) of 100 cm and field sizes of 3 × 3, 5 × 5, 10 × 10, 15 × 15, 20 × 20, 25 × 25, and 30 × 30 cm^2. The field sizes were defined by a pair of sculpted diaphragms mounted orthogonally to MLC. The measurement of the inline and crossline profiles with and without the IQM was performed for field sizes of 3 × 3, 5 × 5, 10 × 10, 20 × 20, and 30 × 30 cm^2 at depths of 5, 10, and 30 cm.

2.B | Measurements of $TPR_{20,10}$, transmission factor, and output factor

$TPR_{20,10}$ was measured in a QWP-07 water phantom (Quolita, Nagano, Japan) using a 0.6 cm^3 TN30013 Farmer-type ionization chamber (PTW Freiburg GmbH, Freiburg, Germany) at a source–chamber distance (SCD) of 100 cm for a field size of 10 × 10 cm^2 with and without the IQM. $TPR_{20,10}$ was obtained from the ratio of the absorbed doses at depths of 20 and 10 cm. The transmission factor and output factor were measured for all energies and field sizes of 3 × 3, 5 × 5, 10 × 10, 15 × 15, 20 × 20, 25 × 25, and 30 × 30 cm^2 with and without the IQM. The field sizes of 5 × 5, 10 × 10, 15 × 15, 20 × 20, 25 × 25, and 30 × 30 cm^2 were measured using the 0.6 cm^3 TN30013 Farmer-type ionization chamber (PTW Freiburg GmbH, Freiburg, Germany) whereas the field size of 3 × 3 cm^2 was measured using a 0.13 cm^3 CC13 compact ionization chamber (IBA Dosimetry GmbH, Schwarzenbruck, Germany). The transmission factor for a field size was defined as the ratio of the ionization charge with the IQM to that without the IQM at a reference depth of 10 cm in the water phantom.[25,26] The output factor for a certain field size with and without the IQM was defined as the ratio of the measured dose for an actual field size in the water phantom and that for a reference field of 10 × 10 cm^2 at a depth of 10 cm.[25] The differences of output factor with and without the IQM were calculated for all energies and field sizes.

2.C | Evaluation of the effect of IQM on beam quality

The influence of the IQM on the surface and build-up region dose was evaluated by the dose difference from the surface (*depth* = 0 cm) to depth of dose maximum (d_{max}) of the PDD curves with and without the IQM.[27] The $PDD_{20,10}$, $TPR_{20,10}$, PDD curves, and inline/crossline profiles, transmission factor, and output factor with and without the IQM were used to assess the effect of the IQM on beam quality of 4-, 6-, 6-MV FFF, and 10-MV X-ray beams beyond d_{max}. The difference between PDD curves and inline/crossline profiles measured with and without IQM should be within ±1%. The differences at the build-up region dose, $PDD_{20,10}$, $TPR_{20,10}$, PDD curves and inline/crossline profiles, and output factor measured with and without the IQM were defined as follows:

$$Difference(\%) = \frac{X_{with\,IQM} - X_{without\,IQM}}{X_{without\,IQM}} \times 100 \quad (1)$$

where $X_{with\,IQM}$ and $X_{without\,IQM}$ are the build-up region dose, $PDD_{20,10}$, $TPR_{20,10}$, PDD curves, crossline and inline profiles, and output factor measured with and without IQM, respectively.

The PDD curves and crossline and inline profiles measured with IQM were compared with the corresponding PDD curves and crossline and inline profiles measured without IQM using a gamma function described by Low et al.[28] We used dose difference (2%) and distance to agreement acceptance criteria (2 mm) for the gamma calculations. The gamma criteria (10% threshold and gamma passing rate above 95% at 2%/2 mm) was used. Local and global dose differences were analyzed for PDD curves and crossline/inline profiles, respectively.

3 | RESULTS

3.A | The effect of IQM on the surface and build-up region dose

Figures 1(a) to 1(d) show the dose differences from the surface to d_{max} of 4-, 6-, 6-MV FFF, and 10-MV X-ray beams for field sizes of 3 × 3, 5 × 5, 10 × 10, 15 × 15, 20 × 20, 25 × 25, and 30 × 30 cm^2 with and without the IQM. The dose differences at build-up region of each energy for each field sizes from 3 × 3 to 30 × 30 cm^2 decreased with increasing depth from the surface to d_{max} and fell to zero at d_{max}. The differences in the surface dose of all energies for field sizes of 3 × 3, 5 × 5, 10 × 10, 15 × 15, 20 × 20, 25 × 25, and 30 × 30 cm^2 with and without the IQM ranged from −1.4% (4-MV) to −2.3% (6-MV FFF), −1.1% (4-MV) to −1.9% (10-MV), −0.4% (6-MV FFF) to −2.2% (10-MV), −0.1% (6-MV) to −1.5% (10-MV), 0.6% (10-MV) to 2.2% (6-MV FFF), 2.4% (4-MV) to 3.7% (10-MV), and 4.6% (4-MV) to 8.7% (10-MV), respectively. The dose difference at the surface with a field size of 30 × 30 cm^2 for the 10-MV X-ray beam was higher than that of the 4-MV, 6-MV, and 6-MV FFF X-ray beams (8.7%, 4.6%, 6.8%, and 6.7%, respectively).

3.B | The effect of IQM on $PDD_{20,10}$, $TPR_{20,10}$, and PDD curves

The differences in $PDD_{20,10}$ for all energies and all field sizes with and without the IQM were less than 0.6% [Fig. 2(a)]. The $TPR_{20,10}$ values determined for all energies for a field size of 10 × 10 cm^2

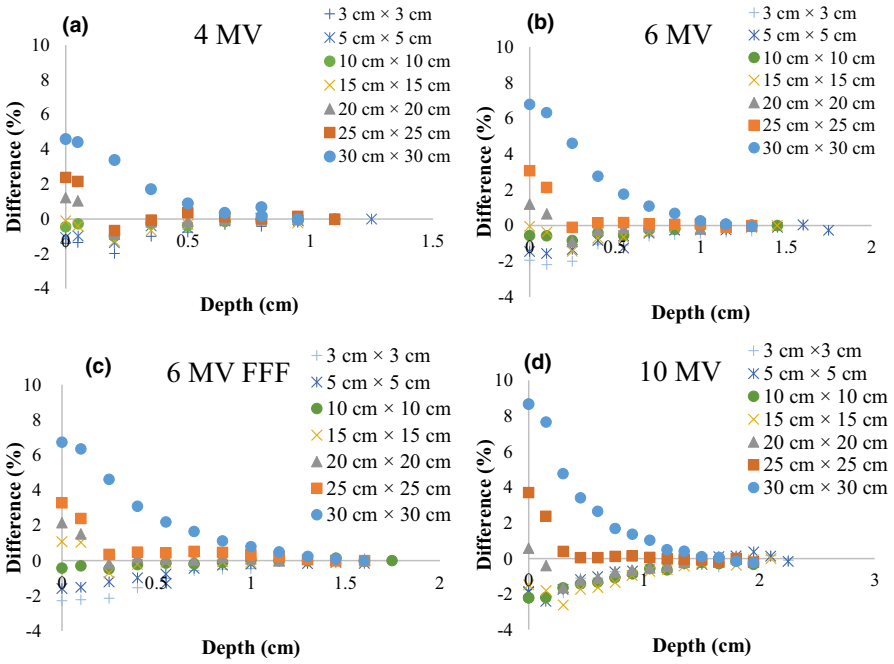

FIG 1. Dose differences from the surface to d_{max} of (a) 4-MV, (b) 6-MV, (c) 6-MV FFF, and (d) 10-MV X-ray beams with and without the IQM for field sizes of 3 × 3, 5 × 5, 10 × 10, 15 × 15, 20 × 20, 25 × 25, and 30 × 30 cm^2 and SSD of 100 cm.

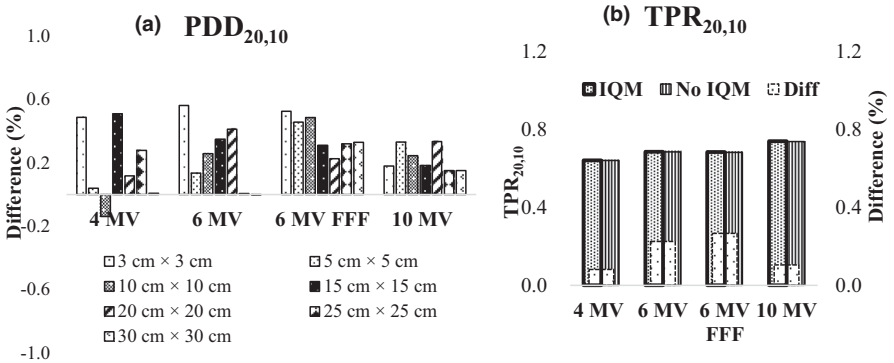

FIG 2. (a) Differences of $PDD_{20,10}$ for field sizes of 3 × 3, 5 × 5, 10 × 10, 15 × 15, 20 × 20, 25 × 25, and 30 × 30 cm^2 at an SSD of 100 cm and (b) comparison of $TPR_{20,10}$ for field size of 10 × 10 cm^2 at a depth of 10 cm and SCD of 100 cm measured with and without the IQM for 4-MV, 6-MV, 6-MV FFF, and 10-MV X-ray beams.

with the IQM agreed with the corresponding $TPR_{20,10}$ data without the IQM within 0.3% [Fig. 2(b)]. The PDD curves and gamma values (2%/2 mm) for PDD curves for the 4-MV, 6-MV, 6-MV FFF, and 10-MV X-ray beams for the seven square fields with sizes of 3 × 3, 5 × 5, 10 × 10, 15 × 15, 20 × 20, 25 × 25, and 30 × 30 cm^2 with and without the IQM are shown in Fig. 3. The gamma values (2%/2 mm) for all energies and field sizes from 3 × 3 to 30 × 30 cm^2 were under 1 except those for the surface of a field size of 30 × 30 cm^2, where the maximum gamma values were 1.64, 2.17, 2.01, and 2.45 for the 4-MV, 6-MV, 6-MV FFF, and 10-MV X-ray beams, respectively. The gamma passing rates (10% threshold) for all energies and field sizes from 3 × 3 to 30 × 30 cm^2 were above 95% at 2%/2 mm.

3.C | The effect of IQM on the crossline and inline profiles

Figures 4 to 8 show the crossline profiles and the corresponding gamma values (2%/2 mm) for crossline profiles of 4-, 6-, 6-MV FFF, and 10-MV X-ray beams with and without the IQM at depths of 5, 10, and 30 cm for the five field sizes of 3 × 3, 5 × 5, 10 × 10, 20 × 20, and 30 × 30 cm^2, respectively. Figures 9 and 10 illustrate the inline profiles and the corresponding gamma values (2%/2 mm) for inline profiles of 4-, 6-, 6-MV FFF, and 10-MV X-ray beams with and without the IQM at depths of 5, 10, and 30 cm for the field sizes of 10 × 10 and 30 × 30 cm^2, respectively. Overall, the crossline and inline profiles measured with the IQM were well matched with the corresponding crossline and inline profiles without the IQM in the central beam region of profiles; however, they were slightly shifted at a depth of 5 cm (within ±1%). At the edge of the dose profiles, the largest differences between the crossline/inline profiles measured with and without the IQM were 15.5% and 17.2% for the crossline and inline profiles, respectively, of the 6-MV FFF X-ray beam for the field size of 30 × 30 cm^2 at a depth of 5 cm [Figs. 8(c) and 10(c)]. The differences at the edge of the crossline profiles for the field size of 30 × 30 cm^2 ranged from 7.4% (10 MV) to 15.5% (6-MV FFF) at a depth of 5 cm, 5.9% (10 MV) to 9.5% (6-MV FFF) at a depth of 10 cm, and 2.4% (6 MV) to 4.2% (6-MV FFF) at a depth of 30 cm (Fig. 8). The differences at the edge of inline profiles for the field size of 30 × 30 cm^2 ranged from 11.2% (4 MV) to

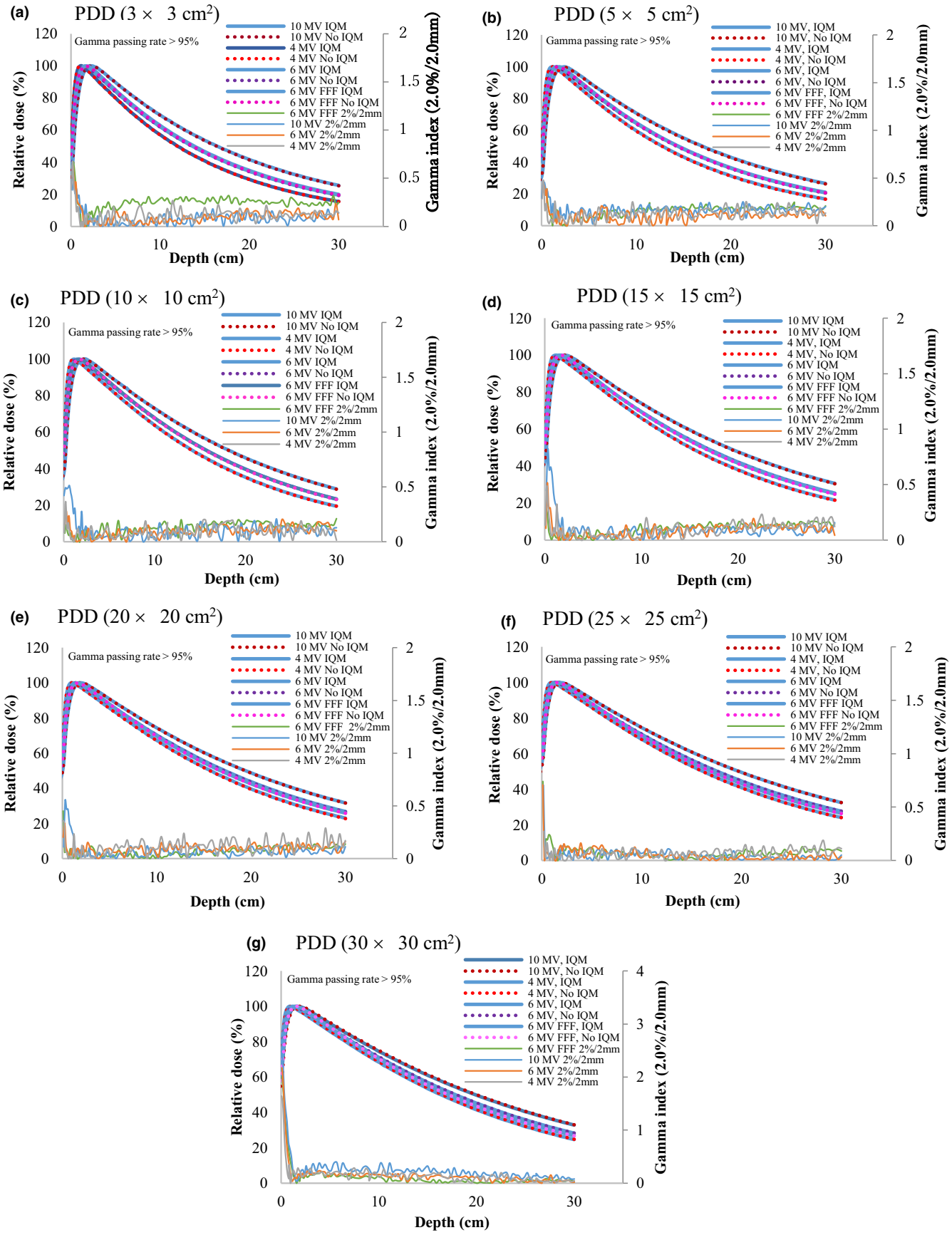

FIG 3. PDD curves and gamma values (2%/2 mm) for PDD of 4-MV, 6-MV, 6-MV FFF, and 10-MV X-ray beams with and without the IQM for field sizes of (a) 3 × 3, (b) 5 × 5, (c) 10 × 10, (d) 15 × 15, (e) 20 × 20, (f) 25 × 25, and (g) 30 × 30 cm^2 and an SSD of 100 cm.

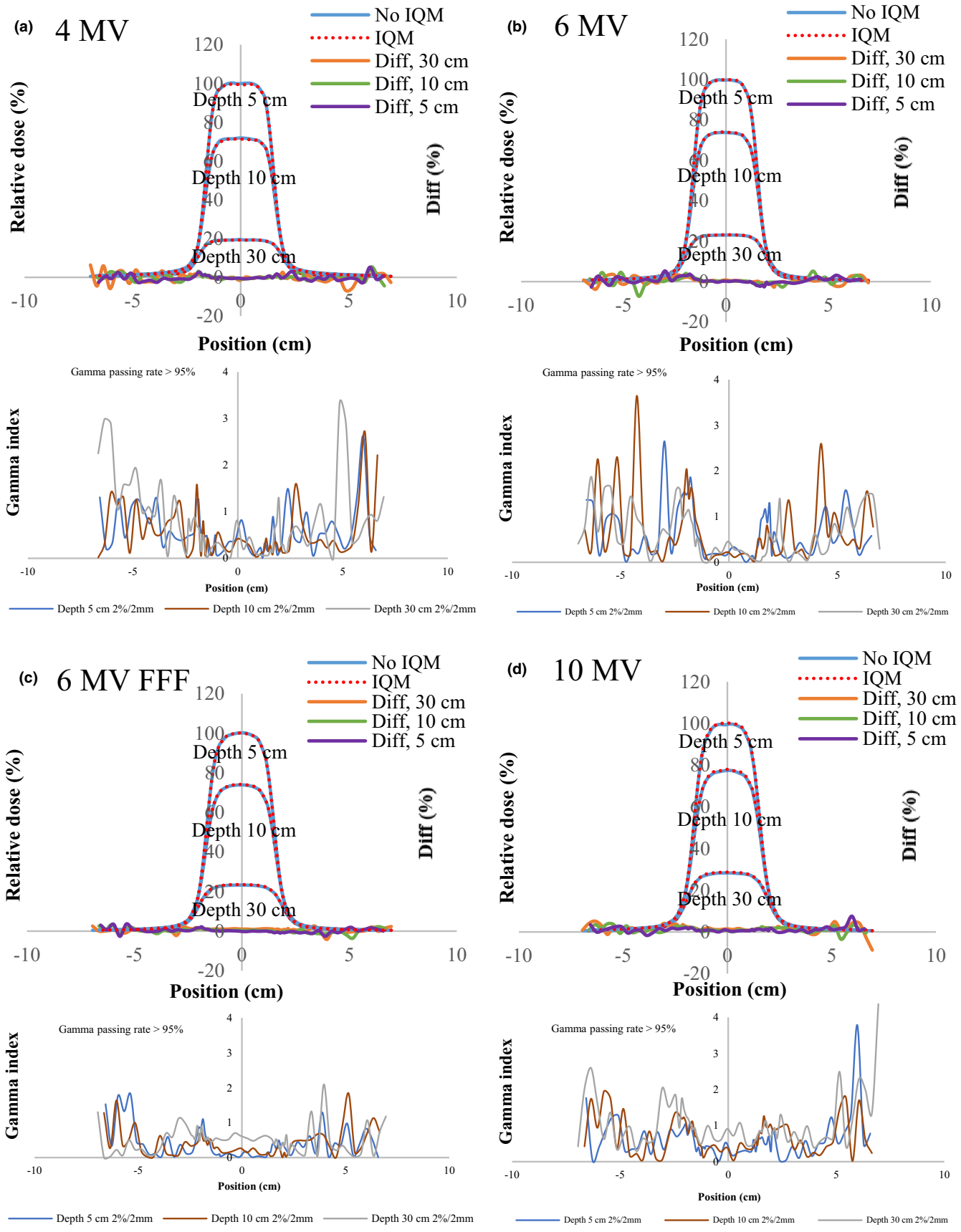

FIG 4. The crossline profiles and gamma values (2%/2 mm) for crossline profiles of (a) 4-MV, (b) 6-MV, (c) 6-MV FFF, and (d) 10-MV X-ray beams with and without the IQM at depths of 5, 10, and 30 cm for a field size of 3 × 3 cm^2 and SSD of 100 cm.

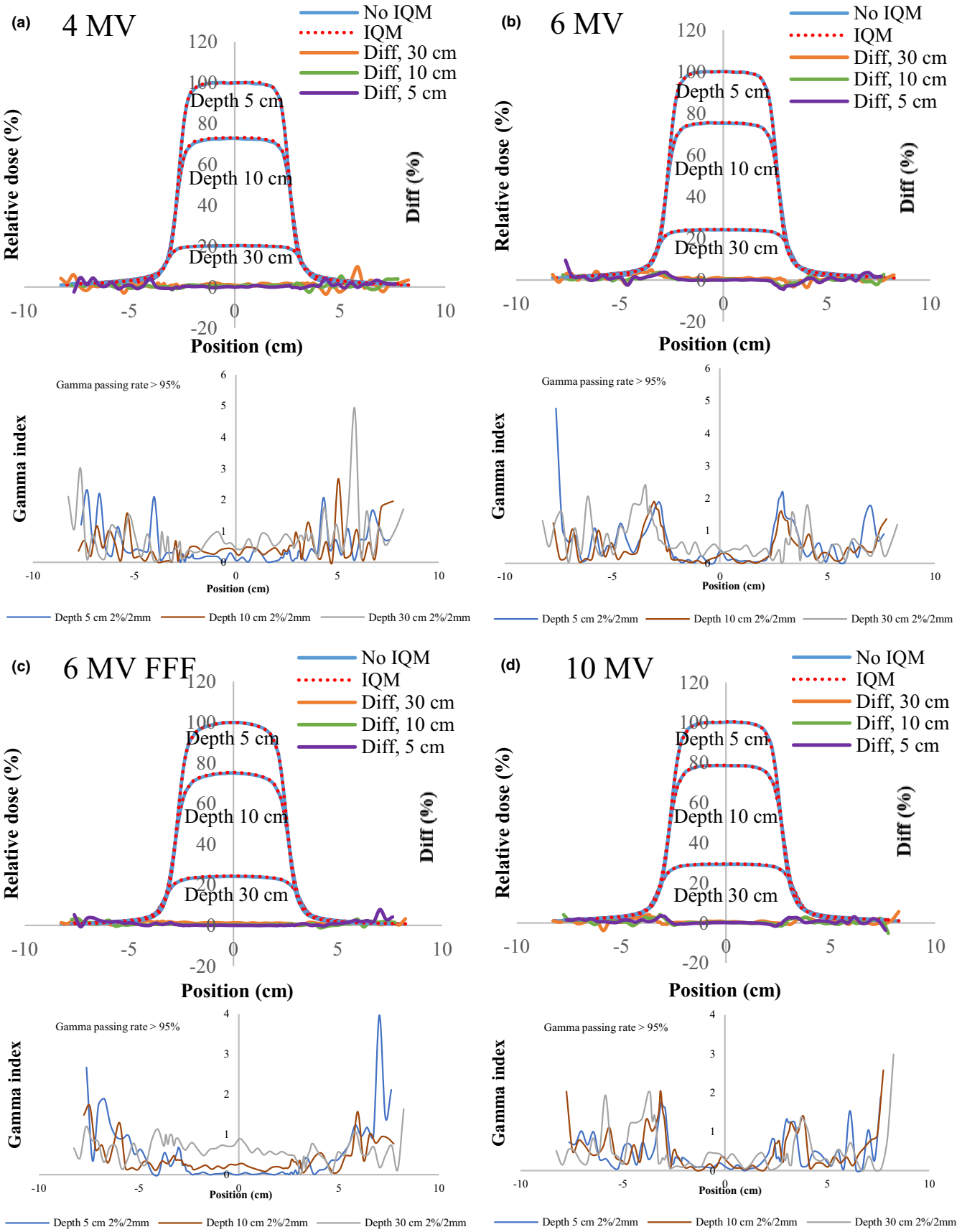

FIG 5. The crossline profiles and gamma values (2%/2 mm) for crossline profiles of (a) 4-MV, (b) 6-MV, (c) 6-MV FFF, and (d) 10-MV X-ray beams with and without the IQM at depths of 5, 10, and 30 cm for a field size of 5 × 5 cm^2 and SSD of 100 cm.

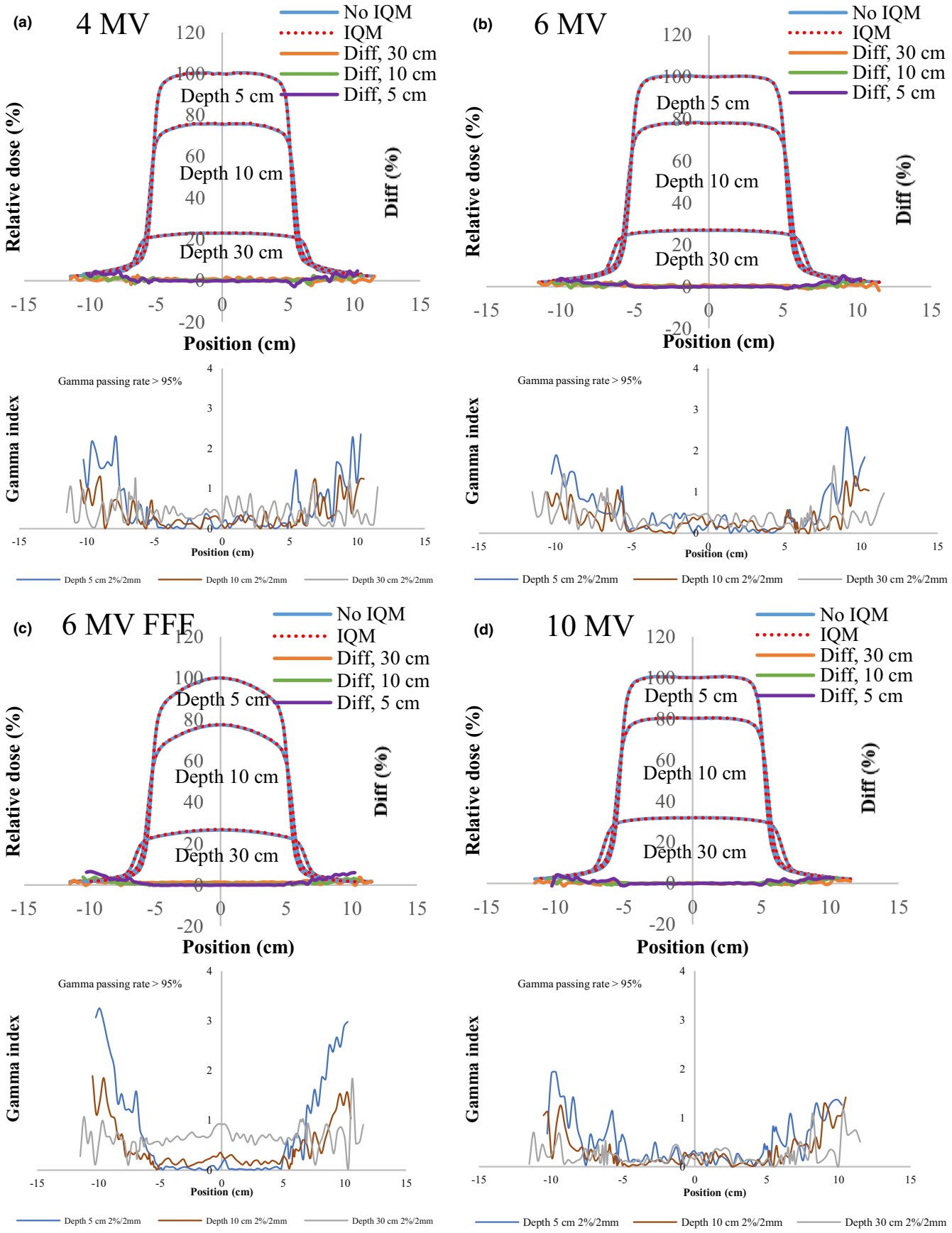

FIG 6. The crossline profiles and gamma values (2%/2 mm) for crossline profiles of (a) 4-MV, (b) 6-MV, (c) 6-MV FFF, and (d) 10-MV X-ray beams with and without the IQM at depths of 5, 10, and 30 cm for a field size of 10 × 10 cm^2 and SSD of 100 cm.

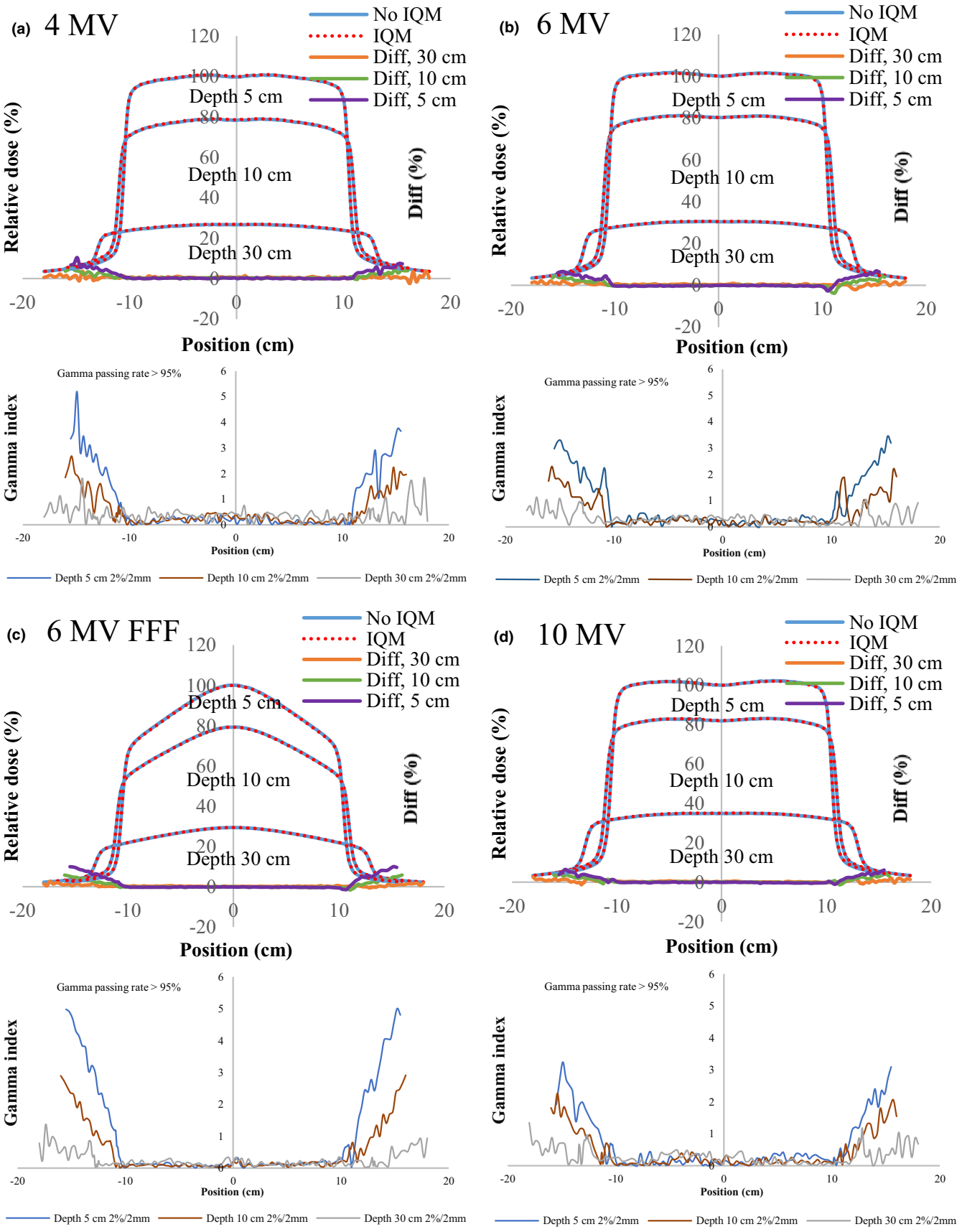

FIG 7. The crossline profiles and gamma values (2%/2 mm) for crossline profiles of (a) 4-MV, (b) 6-MV, (c) 6-MV FFF, and (d) 10-MV X-ray beams with and without the IQM at depths of 5, 10, and 30 cm for a field size of 20 × 20 cm^2 and SSD of 100 cm.

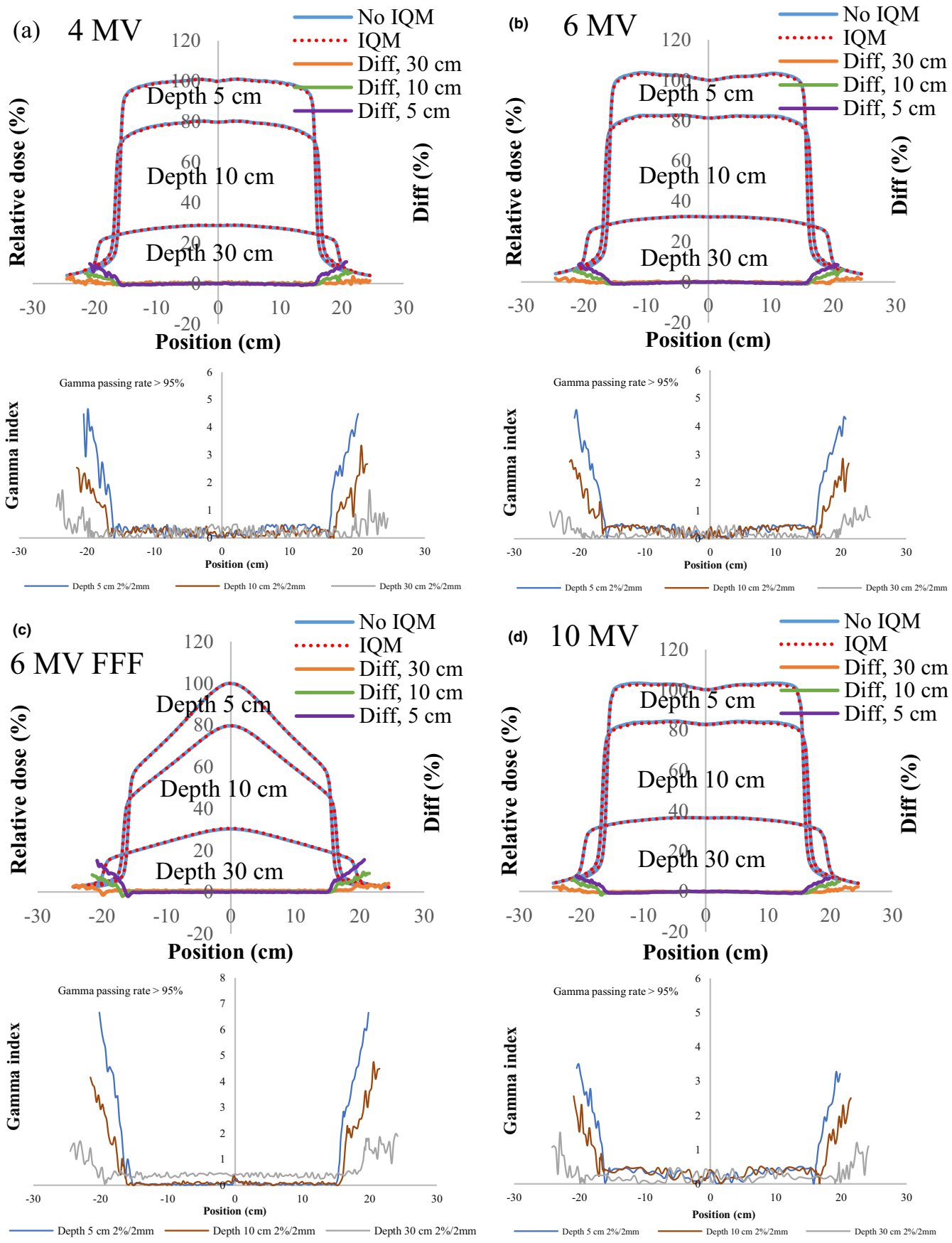

FIG 8. The crossline profiles and gamma values (2%/2 mm) for crossline profiles of (a) 4-MV, (b) 6-MV, (c) 6-MV FFF, and (d) 10-MV X-ray beams with and without the IQM at depths of 5, 10, and 30 cm for a field size of 30 × 30 cm^2 and SSD of 100 cm.

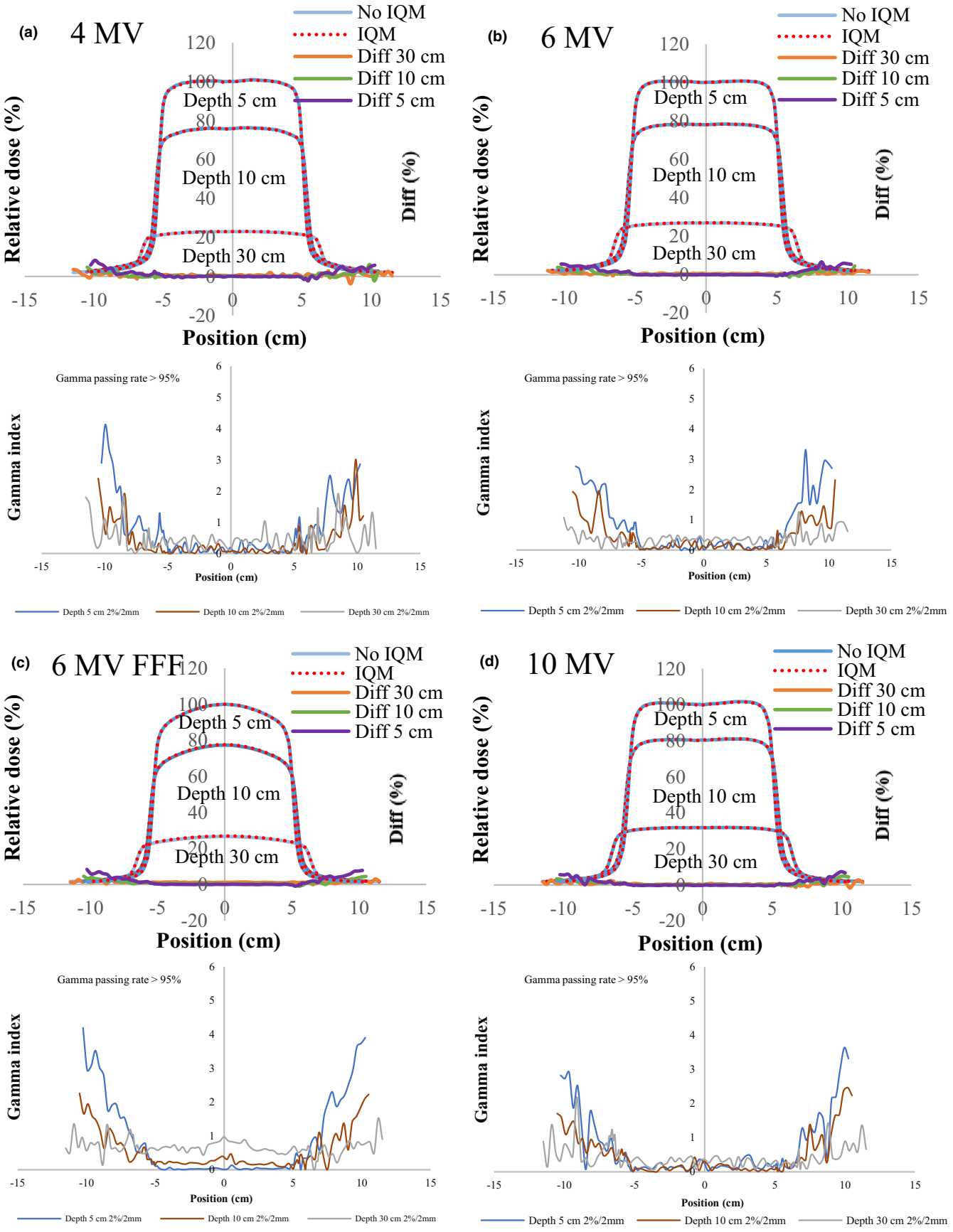

FIG 9. The inline profiles and gamma values (2%/2 mm) for inline profiles of (a) 4-MV, (b) 6-MV, (c) 6-MV FFF, and (d) 10-MV X-ray beams with and without the IQM at depths of 5, 10, and 30 cm for a field size of 10 × 10 cm^2 and SSD of 100 cm.

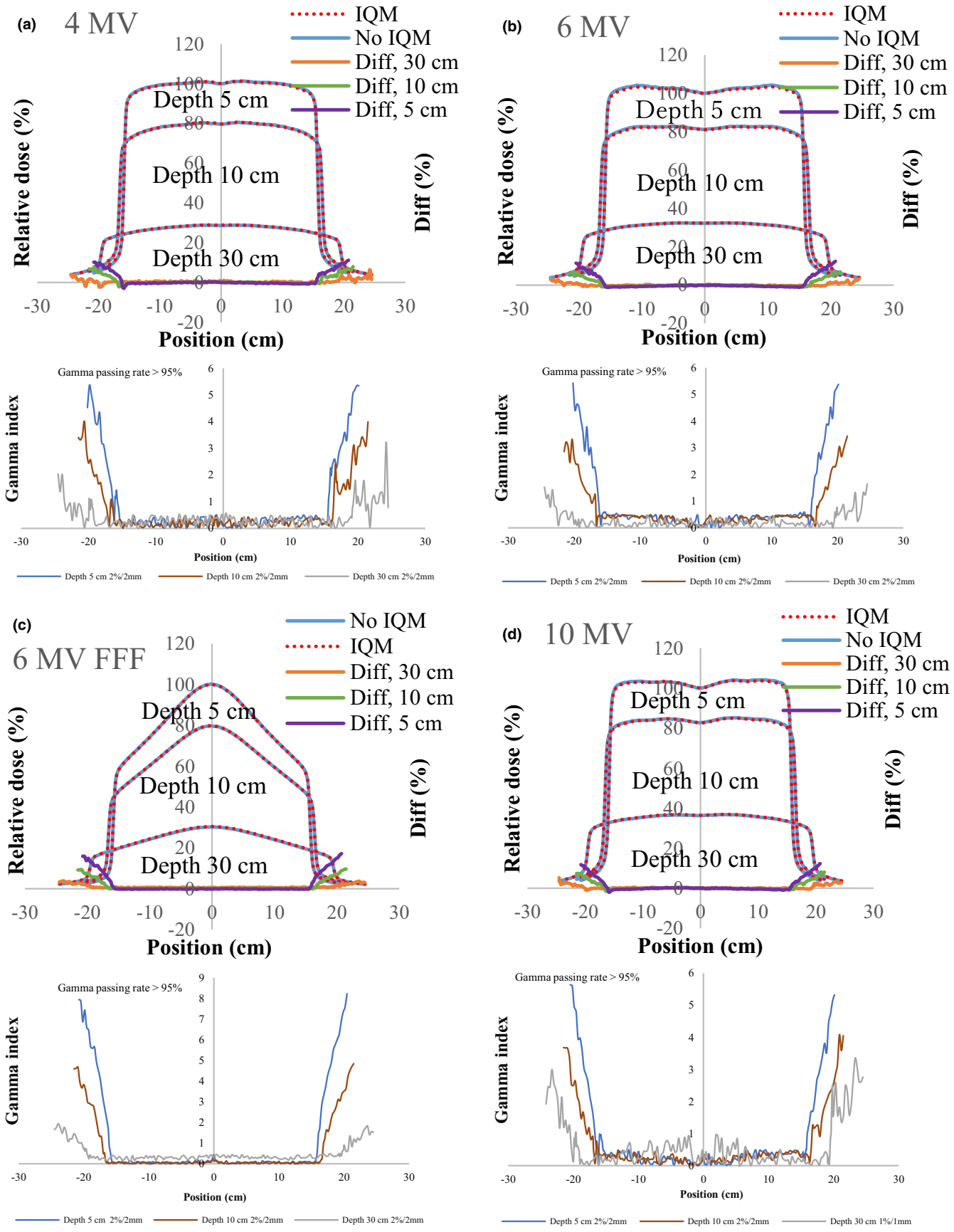

FIG 10. The inline profiles and gamma values (2%/2 mm) for inline profiles of (a) 4-MV, (b) 6-MV, (c) 6-MV FFF, and (d) 10-MV X-ray beams with and without the IQM at depths of 5, 10, and 30 cm for a field size of 30 × 30 cm^2 and SSD of 100 cm.

17.2% (6-MV FFF) at a depth of 5 cm, 6.9% (6 MV) to 9.7% (6-MV FFF) at a depth of 10 cm, and 3.3% (6 MV) to 6.5% (4 MV) at a depth of 30 cm (Fig. 10). By gamma function calculations (2%/2 mm), the crossline/inline profiles measured with IQM showed good agreement with the corresponding crossline/inline profiles measured without IQM in the radiation field regions with gamma values below 1 except those for the edge of crossline/inline profiles. The gamma passing rates (10% threshold) for all energies and field sizes from 3 × 3 to 30 × 30 cm^2 were above 95% at 2%/2 mm. At the edge of crossline/inline profiles, the gamma values at each energy and each field size decreased with increasing of depth from 5 to 30 cm. The gamma values of each energy at the edge of crossline/inline profiles increased with increase of field sizes from 3 × 3 to 30 × 30 cm^2 with largest gamma values (2%/2 mm) of 6.67 and 8.23 for the crossline and inline profiles, respectively, of the 6-MV FFF X-ray beam for field size of 30 × 30 cm^2 at a depth of 5 cm [Fig. 8(c) and 10(c)].

3.D | The effect of IQM on the transmission factors and output factors

The transmission factors for 4-MV, 6-MV, 6-MV-FFF, and 10-MV X-ray beams for field sizes from 3 × 3 to 30 × 30 cm^2 were 0.926–0.933, 0.937–0.941, 0.937–0.939, and 0.949–0.953, respectively [Fig. 11(a)]. The differences between the lowest and highest transmission factors versus field sizes from 3 × 3 to 30 × 30 cm^2 for 4-MV, 6-MV, 6-MV FFF, and 10-MV X-ray beams were 0.009, 0.009, 0.004, and 0.007, respectively. The differences in output factors of all energies for all field sizes with and without the IQM were in the range from −0.8% (4-MV) to 0.5% (10-MV) [Figs. 11(b)–11(e)].

4 | DISCUSSION

4.A | The effect of IQM on the surface and build-up region dose

The results showed that the dose differences at the surface and build-up region depended on the beam energy and field size. The differences were within 3.7% for field sizes from 3 × 3 to 25 × 25 cm^2, whereas the discrepancy for a field size of 30 × 30 cm^2 was up to 8.7%, which was probably because of more collimator scatter when the field size was larger. The presence of the IQM in the beam line increased the dose at the surface and build-up region when the field size was 30 × 30 cm^2 because of electron contamination. The secondary electrons from the IQM

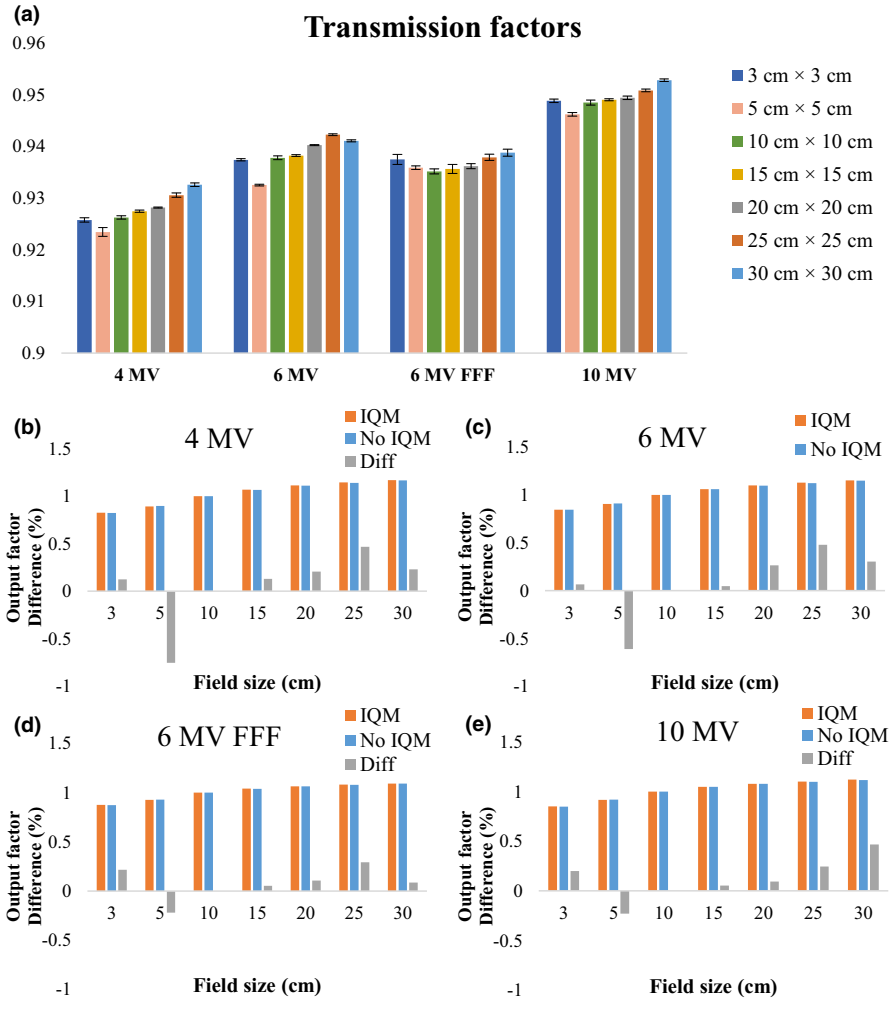

FIG 11. (a) Transmission factors and the differences of output factors for (b) 4-MV, (c) 6-MV, (d) 6-MV FFF, and (e) 10-MV X-ray beams at a depth of 10 cm for field sizes of 3 × 3, 5 × 5, 10 × 10, 15 × 15, 20 × 20, 25 × 25, and 30 × 30 cm^2 and an SCD of 100 cm. The error bars show the standard deviations from five repeated measurements.

interacted with the phantom and decreased with increasing depth.[10,12,29,30] Therefore, the electron contamination in deeper regions was lower compared with that in the surface region.[31,32] The gamma values (2%/2 mm) were <1 except those for the surface of a field size of 30 × 30 cm^2, where the maximum gamma values were 1.64, 2.17, 2.01, and 2.45 for the 4-MV, 6-MV, 6-MV FFF, and 10-MV X-ray beams, respectively. The difference at the surface dose for the field size of 30 × 30 cm^2 increased with beam energy from 4 MV (4.6%) to 10 MV (8.7%). Casar et al.[22] obtained similar results for the difference of surface dose, finding the largest difference of 8.1% for a field size of 20 × 20 cm^2 (10-MV FFF X-ray beam) and within 3.3% for field sizes from 4 × 4 to 15 × 15 cm^2 (6-MV, 10-MV, 15-MV, 18-MV, 6-MV FFF, and 10-MV FFF X-ray beam). The magic plate and Dolphin detector showed an increase of surface dose, with a maximum value of 12.1% at the source to detector distance of 80 cm and 11% at SSD of 80 cm for 30 × 30 cm^2 field size (6-MV X-ray beam), respectively.[10,29] The presence of IBA COMPASS detector in the beam path increased to 8.1% of the surface dose at field size of 20 × 20 cm^2 and SSD of 90 cm (6-MV X-ray beam).[12]

4.B | The effect of IQM on $PDD_{20,10}$, $TPR_{20,10}$, and PDD curves

We found that there was a small difference in $PDD_{20,10}$ values with and without the IQM for all energies and all field sizes (within 0.6%). Because the differences of PDD at a depth of 20 cm for field sizes of 5 × 5, 10 × 10, 25 × 25, and 30 × 30 cm^2 of the 6-MV FFF X-ray beam were larger than those obtained for the other energies, the differences in $PDD_{20,10}$ of the 6-MV FFF X-ray beam for these field sizes were higher than those at the other energies, with the highest value of 0.5% obtained for a field size of 10 × 10 cm^2. Casar and colleagues showed that the largest difference in $PDD_{20,10}$ for a 6-MV FFF X-ray beam was 0.5%.[22] The differences between $TPR_{20,10}$ with and without the IQM did not exceed 0.3%, with the highest value observed for the 6-MV FFF X-ray beam (0.3%) and the lowest value for the 4-MV X-ray beam (0.1%). The differences and gamma values (2%/2 mm) in PDD beyond d_{max} with and without the IQM for all energies and field sizes were within ±1% and below 1, respectively. The gamma passing rates (10% threshold) for all energies and field sizes from 3 × 3 to 30 × 30 cm^2 were above 95% at 2%/2 mm. Islam et al.[9] showed that the differences in PDD in the transient charged particle equilibrium region for a 6-MV X-ray beam were within ±1%.

4.C | The effect of IQM on the crossline and inline profiles

The differences and gamma values (2%/2 mm) in the central region of the dose profiles with and without the IQM for all energies and field sizes were within ±1% and below 1, respectively. The gamma passing rates (10% threshold) for all energies and field sizes from 3 × 3 to 30 × 30 cm^2 were above 95% at 2%/2 mm. Islam et al.[9] showed that the dose profiles at the central region for a 6-MV X-ray beam were within ±1%. However, the differences at the edge of the dose profiles measured with and without the IQM in this study were up to 17.2% for the inline profile (6-MV FFF) and 15.5% for the crossline profile (6-MV FFF) for field size of 30 × 30 cm^2 at a depth of 5 cm. The gamma values at the edge of the dose profiles were up to 4.4 and 5.5 for the crossline and inline profiles, respectively, of the 6-MV FFF X-ray beam for field size of 30 × 30 cm^2 at a depth of 5 cm.

4.D | The effect of IQM on the transmission factors and output factors

When the IQM was placed in the beam path, the beam attenuation of the IQM decreased with increasing X-ray beam energy from 4 to 10 MV and decreased with increasing field size from 3 × 3 to 30 × 30 cm^2. The transmission factors of square fields with sizes from 3 × 3 to 30 × 30 cm for 6-MV, 10-MV, and 6-MV FFF X-ray beam were 0.94, 0.95, and 0.94, respectively. Casar et al.[22] found that mean transmission factors of all square fields from 1 × 1 to 20 × 20 cm^2 for 6-MV, 10-MV, and 6-MV FFF multicenter X-ray beams were 0.94, 0.95, and 0.94, respectively. This study showed that the IQM attenuated the 6-MV beam with a field size of 10 × 10 cm^2 by 6.2%. Islam and co-workers revealed that the IQM attenuated a 6-MV beam with a field size of 10 × 10 cm^2 by 7%.[9]

The differences of output factors varied as a function of the field size and were within ±1% with the lowest values observed for the 6-MV X-ray beam (0.1% for 3 × 3 cm^2) and 6-MV FFF X-ray beam (–0.2%, 0.1%, 0.1%, 0.3%, and 0.1% for 5 × 5, 5 × 15, 20 × 20, 25 × 25, and 30 × 30 cm^2, respectively). The backscatter from the IQM may affect the differences in output factors with and without the IQM. For a field size of 5 × 5 cm^2, the output factors measured with the IQM for all energies were lower than those measured without the IQM. In contrast, for field sizes of 3 × 3, 15 × 15, 20 × 20, 25 × 25, and 30 × 30 cm^2, the output factors measured with the IQM for all energies were higher than those measured without the IQM.

The difference in the surface dose when the field size was 30 × 30 cm^2 for the 6-MV FFF X-ray beam was smaller than those for the 6- and 10-MV X-ray beam because the FFF conditions decreased the electrons contamination.[30] The differences in $PDD_{20,10}$, $TPR_{20,10}$, and crossline/inline profiles of the 6-MV FFF X-ray beam with and without the IQM were larger than those of the conventional flattening filter photon beams (4-, 6-, and 10-MV X-ray beams), whereas the differences in output factors were smaller compared with those obtained for beams with other energies. The flattening filter eliminated the primary photons. Therefore, the edge of the field of the FFF beam received a higher head scatter dose compared with that for the edge of beams with the flattening filter.

The differences in surface and build-up dose, $PDD_{20,10}$, and $TPR_{20,10}$ of the 4-MV X-ray beam with and without the IQM were smaller than those obtained at other energies. However, the beam attenuation of the IQM for the 4-MV X-ray beam was higher than

that of beams with other energies. Therefore, a tray factor should be put into treatment planning systems for dose calculation for the 4-MV X-ray beam. Casar et al.[22] suggested to configure treatment planning system through tray factors or modify output factors for particular beam energy before using IQM in pre- and intra- treatment QA. Therefore, it is necessary to evaluate the commissioning of the IQM device whether the changes in the beam characteristics and output factors could account for the attenuation of IQM. Some papers showed that the IQM system has the potential in its clinical use. Marrazzo et al.[33] reported the IQM detector is a highly sensitive dose-monitoring device for clinical practice of step-and-shoot IMRT plan and found a good correlation between the measured IQM signal and DVH metrics that is useful for identifying clinical action levels. Esposito et al.[20] performed the IQM that is a useful in vivo dosimetry tool with the strengths of real-time monitoring of linac status and can monitor all fractions. The differences in surface and build-up dose, $PDD_{20,10}$, PDD curves, and crossline/inline profiles, and attenuation of the IQM for 6- and 10-MV X-ray beams with and without the IQM were relatively similar to the findings published in previous papers.[9,22,23]

The differences of crossline/inline profiles with and without the IQM increased from the end position of the field width to the end of the crossline/inline profiles, which might be related to reasons such as the radiation component of secondary electrons, beam hardening effect, and backscattered radiation from the aluminum plates (alloy 6061) of the IQM. Moreover, the Infinity Agility MLC system has a pair of backup jaws that are orthogonal to the direction of leaf motion. Therefore, the scatter from sculpted field-length defining collimators may affect the edge of the inline profile. The differences and gamma values at the outside region of the fields of crossline/inline profiles with and without the IQM decreased with increasing depth in the order of 5 to 10 to 30 cm, which was probably caused by the presence of contaminating electrons from the treatment head and IQM at shallow depth.[29] As a limitation of this study, the cause of the differences at the toe of crossline/inline profiles with and without the IQM is still unclear. Therefore, it is necessary to evaluate photon energy properties with and without the IQM, factors influencing beam characteristics, and backscatter contribution using Monte Carlo simulations and to verify the simulation results with the measured data. The differences at the toe of crossline/inline profiles measured with and without the IQM showed whether the presence of the IQM affects MLC-generated photon fluence in IMRT technique dosimetry. Therefore, the ability of using the IQM detector in verification of IMRT delivery should be investigated.

5 | CONCLUSION

We evaluated the difference in the beam quality measured with and without an IQM and found the field-size and beam-energy dependence of the IQM. The influence of IQM on the beam quality (in particular 4-MV X-ray has not verified before) was tested and introduced a slight beam perturbation at the surface and build-up region and the edge of the crossline/inline profiles. To use IQM in pre- and intra-treatment QA, a tray factor should be put into treatment planning systems for the dose calculation for the 4-, 6-, 10-MV, and 6-MV flattening filter-free photon beams to compensate for the attenuation of the IQM detector.

ACKNOWLEDGMENTS

We thank Natasha Lundin, PhD, from Edanz Group (HYPERLINK "http://www.edanzediting.com/ac" www.edanzediting.com/ac) for editing a draft of this manuscript.

CONFLICT OF INTEREST

This study was a collaborative research project with APEX Medical, Inc."

AUTHOR CONTRIBUTION STATEMENT

Trang Hong Thi Nguyen, Conceived and designed the analysis, collected the data, contributed data or analysis tools, performed the analysis, wrote the paper, and revised the paper. Haruna Yokoyama; Collected the data, contributed data or analysis tools, performed the analysis, reviewed and revised the paper. Hironori Kojima, Collected the data, contributed data or analysis tools, performed the analysis, reviewed and revised the paper. Naoki Isomura, Collected the data, contributed data or analysis tools, performed the analysis, reviewed and revised the paper. Akihiro Takemura, Collected the data, contributed data or analysis tools, performed the analysis, reviewed and revised the paper. Shinichi Ueda, Collected the data, contributed data or analysis tools, performed the analysis, reviewed and revised the paper. Kimiya Noto, Collected the data, contributed data or analysis tools, performed the analysis, reviewed and revised the paper.

REFERENCES

1. Herzen J, Todorovic M, Cremers F, et al. Dosimetric evaluation of a 2D pixel ionization chamber for implementation in clinical routine. *Phys Med Biol*. 2007;52:1197–1208.
2. Kron T. Thermoluminescence dosimetry and its applications in medicine—part 2: history and applications. *Austr Phys Eng Sci Med*. 1995; 18:1–25.
3. Zhuang AH, Olch AJ. Validation of OSLD and a treatment planning system for surface dose determination in IMRT treatments. *Med Phys*. 2014;41:081720.
4. Ju SG, Ahn YC, Huh SJ, et al. Film dosimetry for intensity modulated radiation therapy: dosimetric evaluation. *Med Phys*. 2002;29:351–355.
5. Nelms BE, Zhen H, Tomé WA. Per-beam, planar IMRT QA passing rates do not predict clinically relevant patient dose errors. *Med Phys*. 2011;38:1037–1044.
6. Carrasco P, Jornet N, Latorre A, Eudaldo T, Ruiz A, Ribas M. 3D DVH-based metric analysis versus per-beam planar analysis in IMRT pretreatment verification. *Med Phys*. 2012;39:5040–5049.
7. IAEA Human Health Reports No. 7. *Record and Verify Systems for Radiation Treatment of Cancer: Acceptance Testing, Commissioning and Quality Control*. Vienna: International Atomic Energy Agency; 2013.

8. The Royal College of Radiologists, Society and College of Radiographers, Institute of Physics and Engineering in Medicine. *On Target: Ensuring Geometric Accuracy in Radiotherapy*. London: The Royal College of Radiologist; 2008.
9. Islam MK, Norrlinger BD, Smale JR, et al. An integral quality monitoring system for real-time verification of intensity modulated radiation therapy. *Med Phys*. 2009;36:5420–5428.
10. Wong JHD, Fuduli I, Carolan M, et al. Characterization of a novel two dimensional diode array the 'magic plate' as a radiation detector for radiation therapy treatment. *Med Phys*. 2012;39:2544–2558.
11. Poppe B, Looe HK, Chofor N, Ruhmann A, Harder D, Willborn KC. Clinical performance of a transmission detector array for the permanent supervision of IMRT deliveries. *Radiother Oncol*. 2010;95:158–165.
12. Venkataraman S, Malkoske KE, Jensen M, Nakonechny KD, Asuni G, McCurdy BM. The influence of a novel transmission detector on 6 MV x-ray beam characteristics. *Phys Med Biol*. 2009;54:3173–3183.
13. IAEA Human Health Reports No. 8. *Development of Procedures for In Vivo Dosimetry in Radiotherapy*. Vienna: International Atomic Energy Agency; 2013.
14. Poppe B, Thieke C, Beyer D et al DAVID—a translucent multi-wire transmission ionization chamber for in vivo verification of IMRT and conformal irradiation techniques. *Phys Med Biol*. 2006;51:1237–1248.
15. Goulet M, Gingras L, Beaulieu L. Real time verification of multileaf collimator driven radiotherapy using a novel optical attenuation based fluence monitor. *Med Phys*. 2011;38:1459–1467.
16. Litzenberg DW, Moran JM, Fraass BA. Verification of dynamic and segmental IMRT delivery by dynamic log file analysis. *J Appl Clin Med Phys*. 2002;3:63–72.
17. Piermattei A, Fidanzio A, Stimato G, et al. In vivo dosimetry by an aSi-based EPID. *Med Phys*. 2006;33:4414–4422.
18. Ng JA, Booth JT, Poulsen PR, et al. Kilovoltage intra-fraction monitoring for prostate intensity modulated arc therapy: first clinical results. *Int J Radiat Oncol Biol Phys*. 2012;84:e655–e661.
19. Ravkilde T, Skouboe S, Hansen R, et al. First online real-time evaluation of motion-induced 4D dose errors during radiotherapy delivery. *Med Phys*. 2018;45:3893–3903.
20. Esposito M, Villaggi E, Bresciani S, et al. Estimating dose delivery accuracy in stereotactic body radiation therapy: a review of in-vivo measurement methods. *Radiother Oncol*. 2020;149:158–167.
21. Saito M, Sano N, Shibata Y, et al. Comparison of MLC error sensitivity of various commercial devices for VMAT pre-treatment quality assurance. *J Appl Clin Med Phys*. 2018;19:87–93.
22. Casar B, Pasler M, Wegener S, et al. Influence of the integral quality monitor transmission detector on high energy photon beams: a multi-centre study. *Z Med Phys*. 2017;27:232–242.
23. Hoffman D, Chung E, Hess C, Stern R, Benedict S. Characterization and evaluation of an integrated quality monitoring system for online quality assurance of external beam radiation therapy. *J Appl Clin Med Phys*. 2017;18:40–48.
24. Takahashi K, Morota M, Kagami Y, et al. Prospective study of postoperative whole breast radiotherapy for Japanese large-breasted women: a clinical and dosimetric comparisons between supine and prone positions and a dose measurement using a breast phantom. *BMC Cancer*. 2016;16:757.
25. Indra JD, Chee WC, Ronald JW, et al. Accelerator beam data commissioning equipment and procedures: report of the TG-106 of the Therapy Physics Committee of the AAPM. *Med Phys*. 2008;35:4186–4215.
26. Sharma SC, Johnson MW. Recommendations for measurement of tray and wedge factors for high energy photons. *Med Phys*. 1994;21:573–575.
27. Podgorsak EB. *Radiation Oncology Physics: A Handbook for Teachers and Students*. Vienna: International Atomic Energy Agency; 2005. ISBN 978-9201073044.
28. Low DA, Harms WB, Mutic S, Purdy JA. A technique for the quantitative evaluation of dose distributions. *Med Phys*. 1998;25:656–661.
29. Thoelking J, Sekar Y, Fleckenstein J, Lohr F, Wenz F, Wertz H. Characterization of a new transmission detector for patient individualized online plan verification and its influence on 6MV X-ray beam characteristics. *Z Med Phys*. 2016;26:200–208.
30. Nilsson B, Brahme A. Electron contamination from photon beam collimators. *Radiother Oncol*. 1986;5:235–244.
31. Nilsson B, Brahme A. Absorbed dose from secondary electrons in high energy photon beams. *Phys Med Biol*. 1979;24:901–912.
32. Medina AL, Teijeiro A, Garcia J, et al. Characterization of electron contamination in megavoltage photon beams. *Med Phys*. 2005;32:1281–1292.
33. Marrazzo L, Arilli C, Pasler M, et al. Real-time beam monitoring for error detection in IMRT plans and impact on dose-volume histograms: a multi-center study. *Strahlenther Onkol*. 2018;194:243–254.